



New Tools for Terrain Gravimetry
NEWTON-g
Project number: 801221

Deliverable 4.4

Pilot phase of data analysis

Lead beneficiary:	Koninklijk Nederlands Meteorologisch Instituut
Dissemination level:	Public
Version:	FINAL



NEWTON-g has received funding from the EC's Horizon 2020 programme, under the FETOPEN-2016/2017 call (Grant Agreement No 801221)

Document Information

Grant Agreement Number	801221
Acronym	NEWTON-g
Start date of the project	1 June 2018
Project duration (months)	48 (extended to 54)
Deliverable number	D4.4
Deliverable Title	Pilot phase of data analysis
Due date of deliverable	31/05/2022
Actual submission date	24/10/2022
Lead Beneficiary	Koninklijk Nederlands Meteorologisch Instituut (KNMI)
Type	R: Document, report
Dissemination level	PU - Public
Work Package	WP4 – Data analysis

Version	Date	Author	Comments
v.0	22/09/2022	M. Koymans (KNMI)	Creation
v.1	18/10/2022	D. Carbone (INGV)	Revision
v.2	20/10/2022	M. Koymans (KNMI), E. de Zeeuw - van Dalssen, A. Prasad	Revision
Final	24/10/2022	M. Koymans (KNMI), E. de Zeeuw - van Dalssen, D. Carbone	Validation

TABLE OF CONTENTS

1 Overview and scope4

2 History of devices deployment under NEWTON-g5

3 Analysis of data from MEMS gravimeters6

 3.1 RP1.1 (SLN station) 6

 3.2 Wee-g1 (PDN station) 7

 3.3 Wee-g7 (EBEL station) 8

 3.4 Wee-g6 (ECPN station) 8

 3.5 General remarks 9

4 Analysis of data from AQG-B03 and comparison with other gravity data11

 4.1 Introduction 11

 4.2 Comparison with data from other gravimeters on Mt. Etna 11

 4.3 Data inversion 11

5 Concluding remarks13

References14

1 Overview and scope

The main target of NEWTON-g has been the development and field test of new instrumentation for terrain gravimetry. In particular, the project has aimed to field-test, in the summit active zone of Mt. Etna, a system for continuous measurements (the “gravity imager”), including an array of MEMS-based relative devices (Wee-g gravimeters) anchored to a quantum gravimeter (AQG-B), the latter providing the absolute gravity reference for the gravity imager (Carbone et al., 2020).

Due to the COVID-19 pandemic, it was not possible to carry out the project activities as originally planned. In particular, strong restrictions in country-wide working conditions severely limited the ability of the UNIGLA team to carry out the needed R&D and testing and to deliver the planned batch of Wee-g devices for installation on Mt. Etna (see D3.4).

Conversely, the AQG-B was transported to Italy and deployed at Mt. Etna in the summer of 2020 (Antoni-Micollier et al., 2022), in keeping with the original plan (D3.4).

This document was originally meant to report on the preliminary joint analysis of the signals produced by the NEWTON-g’s gravity imager during the pilot phase, after installation. Nevertheless, the above issues imply that a measurement system with the desired characteristics is not yet operational on Mt. Etna. In the following, we thus review the results from the field deployments on Mt. Etna, that were accomplished during the last two years, with a special emphasis on the possibilities of continuous volcano gravimetry.

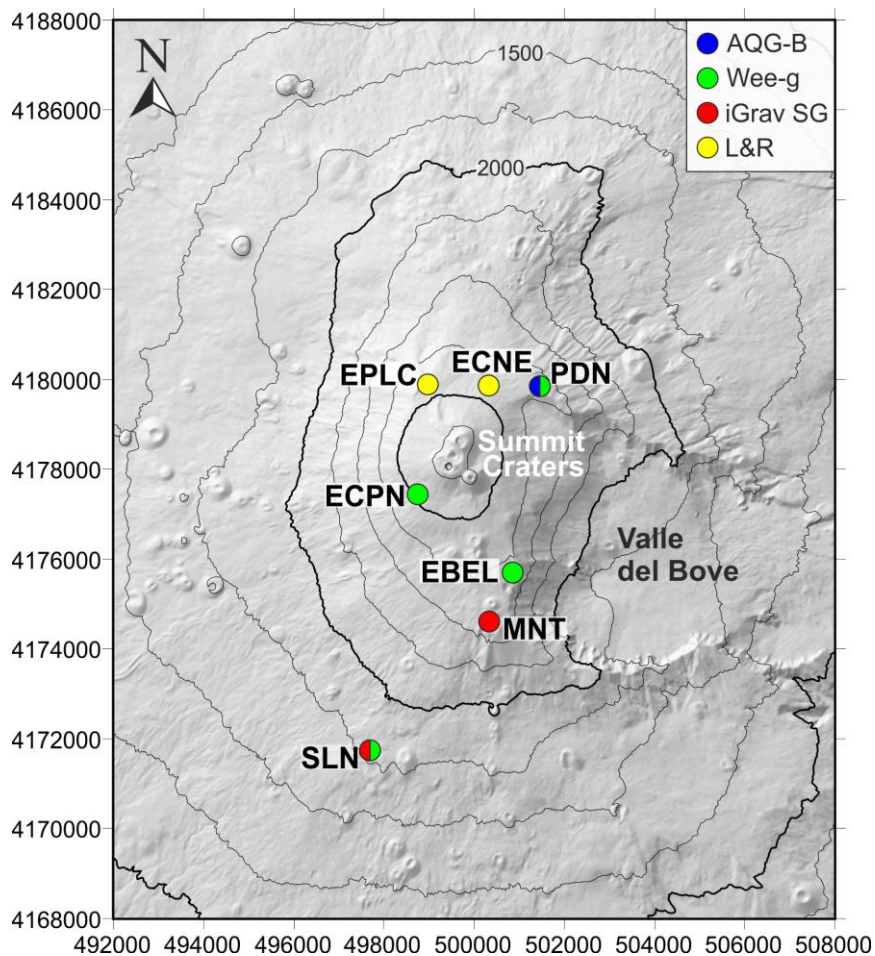


Figure 1 – Sketch map showing the position of the AQG-B quantum gravimeter (blue dot) and Wee-g MEMS devices (green dots) that were installed at Mt. Etna in the framework of NEWTON-g. Also shown are the positions of (i) the iGrav SG in Mt. Etna’s monitoring system (red dots) and the L&R spring gravimeters that were deployed during the summer of 2022. Markers with a mixed color represent sites where different instruments are co-located.

2 History of devices deployment under NEWTON-g

At the end of July 2020, AQG-B#03 was installed in the facilities of the Pizzi Deneri volcanological observatory (PDN; Fig. 1), at 2800 m elevation and 2.5 km from the summit active craters of Mt. Etna. The instrument acquired a 4-month time series in 2020 (August – December; Antoni-Micollier et al., 2022) and a 6.5-month time series in 2021 (late-May – early-December). Up to date, it has not been possible to acquire data during winter, due to failures of the hybrid power supply system of the gravimeter (see D2.6). In May 2022, the AQG-B was sent back to iXblue’s premises (Talence, France) for a few weeks, in order to perform upgrades on the system. The gravimeter was redeployed at PDN in late July 2022 and has recorded data without major interruptions since then. The first prototype of Wee-g was deployed on Mt. Etna in August 2021, in the facilities of the Serra La Nave astrophysical observatory (SLN; Fig. 1), at 1730 m elevation and ~6.5 km from the summit craters. This device, referred to as RP1.1 (“rapid prototype”), does not have all the hardware features of the standard Wee-g devices that have been designed and developed as part of NEWTON-g (see D2.5 and D2.6). Acquisition with RP1.1 at SLN is still ongoing at the time of the present writing (October 2022).

During the summer of 2022, three other Wee-gs were installed at Mt. Etna, at elevations ranging between 2600 and 3000 m. Wee-g#1 was deployed at PDN (Fig. 1), side-by-side with the AQG-B. Wee-g#6 was installed in a site called Cratere del Piano (ECPN; Fig. 1), which is one of the uppermost places with installation facilities on Mt. Etna (i.e., seismic and GPS stations belonging to the monitoring network of INGV-OE). ECPN is located at 2990 m elevation and is only ~1 km away from the summit craters. Finally, Wee-g#7 was installed at a site on the southern slope of the volcano called Belvedere (EBEL; Fig. 1). EBEL is at 2660 m elevation and 2.9 km from the summit craters.



Figure 2 – Deployment of Wee-g7 at EBEL station. The instrument is transported to the installation site upside-down, inside a padded box (left); it is then placed inside the sensor box of the MEMS station (middle; Carbone et al., 2020) and leveled by one operator, while the other checks the effect of turning the adjustable feet of the device through the GUI of the control software (right). The summit craters of Mt. Etna are visible in the background of the picture on the left.

At both ECPN and EBEL, complete MEMS station infrastructures (D3.3; D3.4; Carbone et al., 2020) were installed to (i) protect sensor and electronics from environmental damage and (ii) allow data acquisition, local storage and transmission (Fig. 2). To work properly, Wee-gs need to be thermalised (i.e., brought to required internal operational temperature). The dates when the three Wee-gs installed in 2022 were thermalized and started acquiring gravity data are reported in Table 1.

In order to provide more context for the NEWTON-g deployments, two LaCoste and Romberg spring gravimeters (G models) were also installed on Mt. Etna in June 2022. They were installed at two sites called Cratere di NE (ECNE; L&R G-1190) and Punta Lucia (EPLC; L&R G-594), which are, respectively (Fig. 1), at 2900 m elevation (~1500 m from the summit craters) and 2920 m elevation (1600 m from the summit craters)

3 Analysis of data from MEMS gravimeters

3.1 RP1.1 (SLN station)

A long time series is now available from RP1.1 at SLN (Fig. 1). Data collected in 2022 are shown in Fig 3. The signal is affected by a drift whose linear component is on the order of 140 $\mu\text{Gal/day}$ and by the marked anti-correlation with atmospheric pressure already evidenced in D2.6. Once data are band-pass filtered, a relatively tight correlation with the Earth tide signal appears (corr. factor up to 0.96; Fig. 4).

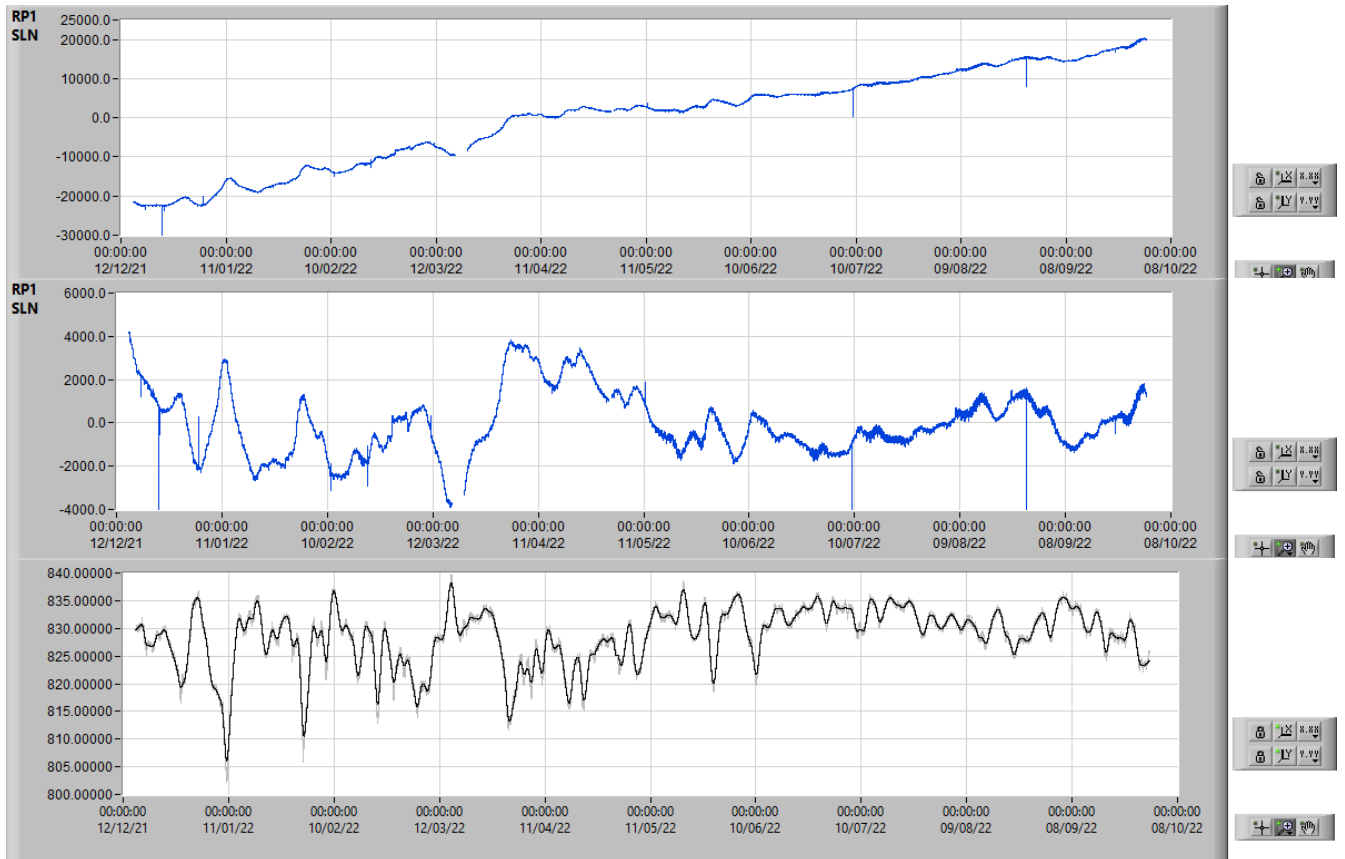


Figure 3 - RP1.1 at SLN. Top: raw gravity. Middle: gravity data after removal of a low-degree polynomial fit. Bottom: atm. pressure

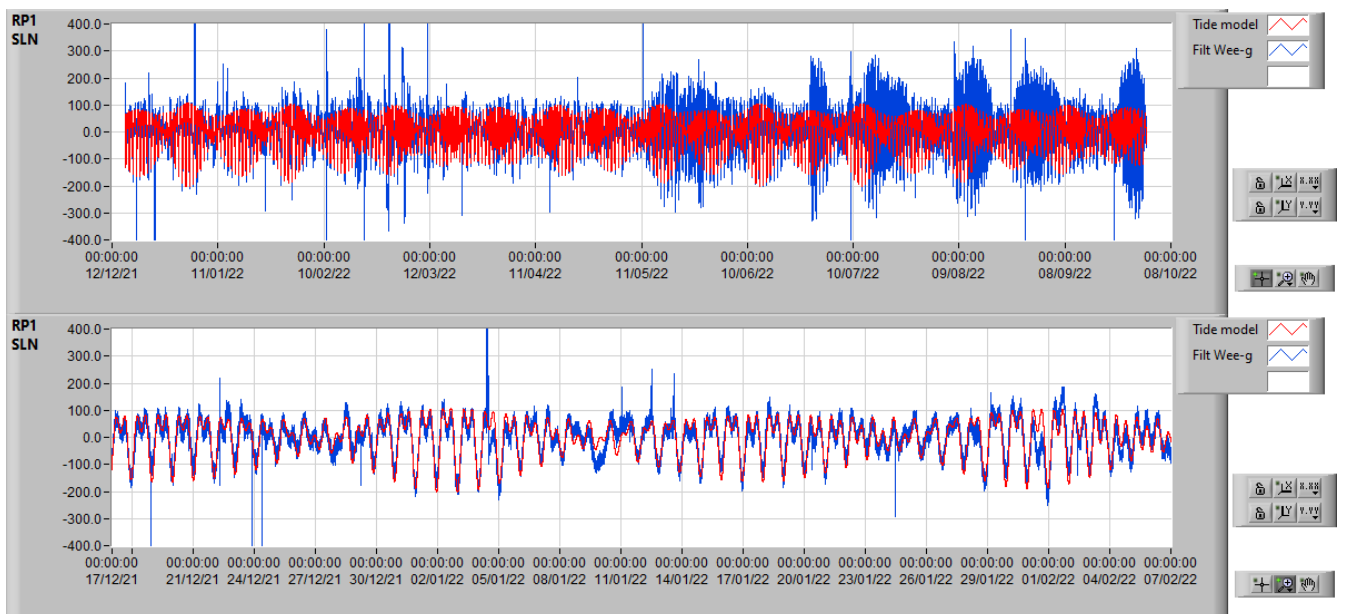


Figure 4 - RP1.1 at SLN. Top: band-pass filtered gravity data (blue) and Earth tide model (red). Bottom: detail of the same plot.

3.2 Wee-g1 (PDN station)

The overall linear drift on data from Wee-g1 at PDN (Fig. 1) is on the order of 80 $\mu\text{Gal}/\text{day}$ and most of the longer-term component is removed through a 2nd degree polynomial fit (residuals within about $\pm 500 \mu\text{Gal}$; Fig. 5). Also in this case, a tight (anti)correlation is observed with atmospheric pressure (Fig. 5).

Unexpectedly, the correlation between band-pass filtered Wee-g signal and Earth tide is much worse than in the case of the RP1.1 signal: the correlation factor is never higher than 0.7 (Fig. 6).

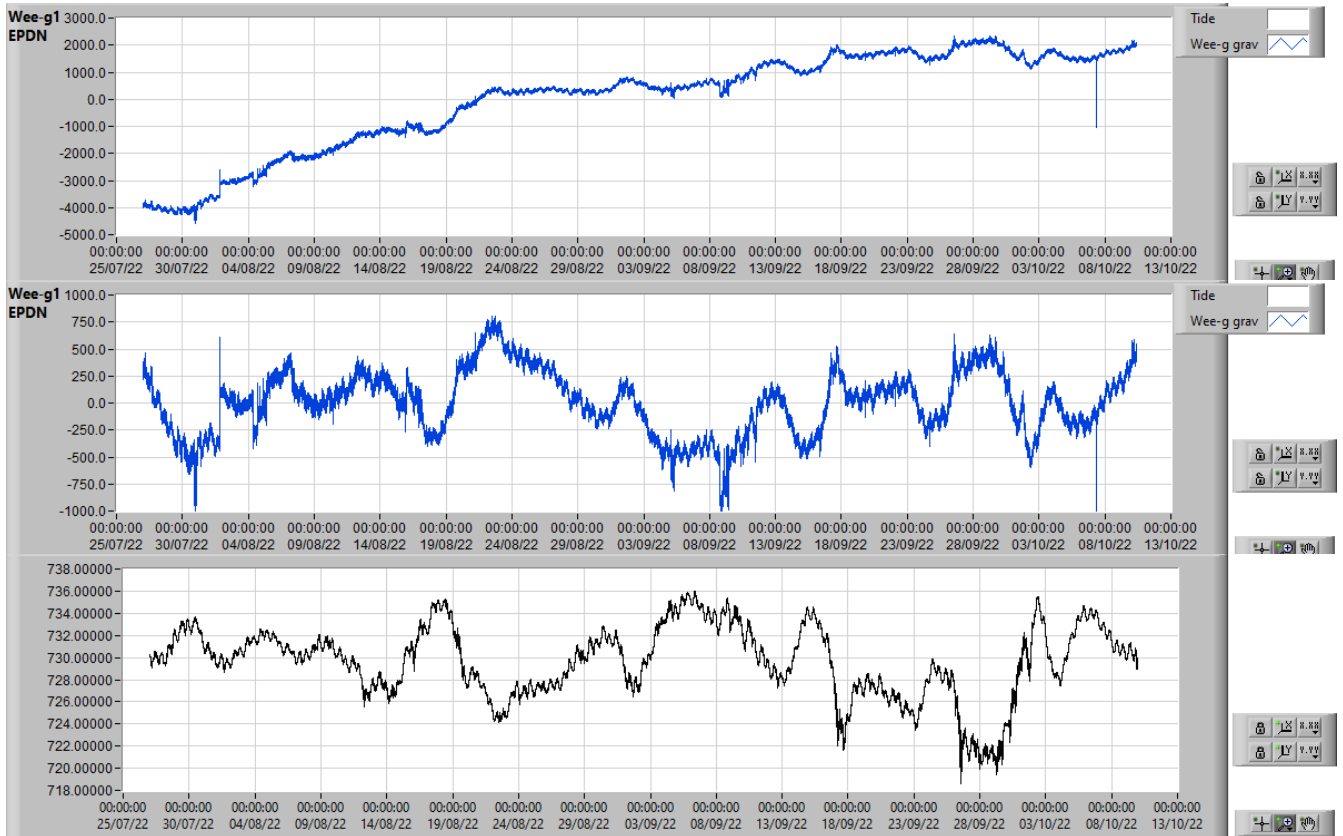


Figure 5 - Wee-g1 at EPDN. Top: raw gravity data. Middle: gravity data after removal of a 2nd-degree polynomial fit. Bottom: Pressure

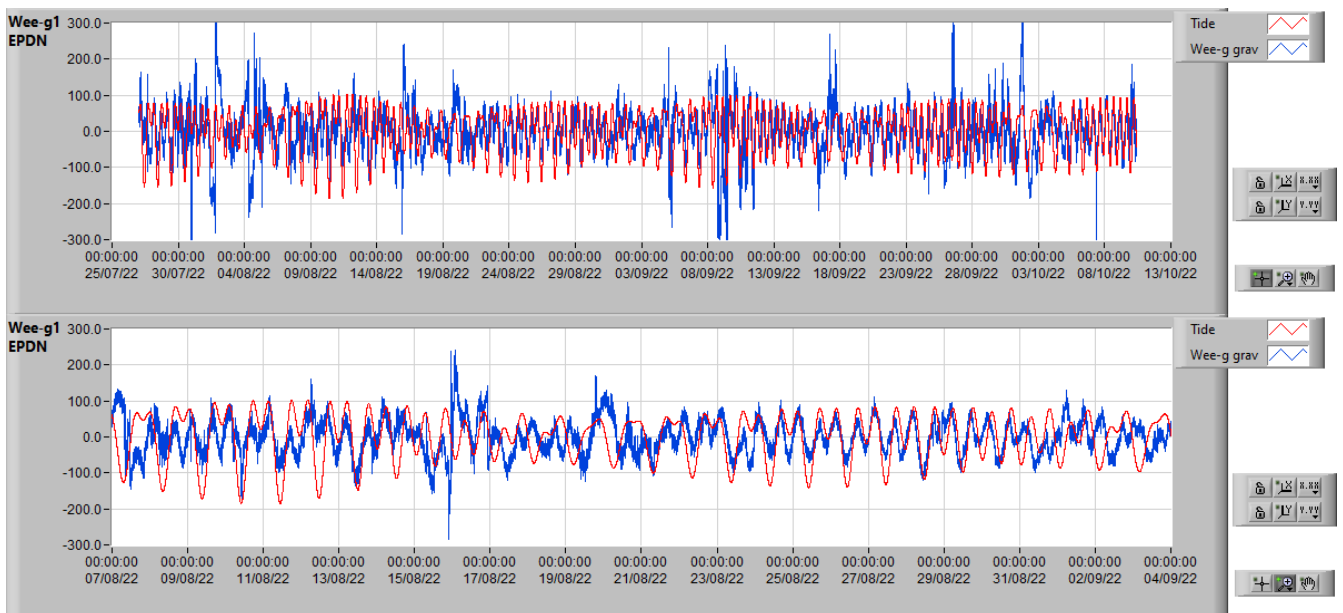


Figure 6 - Wee-g1 at EPDN. Top: band-pass filtered gravity data (blue) and Earth tide model (red). Bottom: detail of the same plot.

3.3 Wee-g7 (EBEL station)

The signal from Wee-g7 at EBEL (Fig. 1) is affected by a strong linear drift, overall, on the order of 3 mGal/day (Fig. 7). However, the rate slows down throughout the available period (mid-September – early October), from about 6 to about 1.3 mGal/day. Most of the longer-term component is removed through a 3rd-order polynomial fit (residuals within +/- 400 μ Gal; Fig. 6). No correlation seems to exist between the signal from Wee-g7 and the atmospheric pressure. Also for Wee-g7, the correlation between band-pass filtered gravity signal and Earth tide is worse than expected, in general within about 0.8 (Fig. 8).

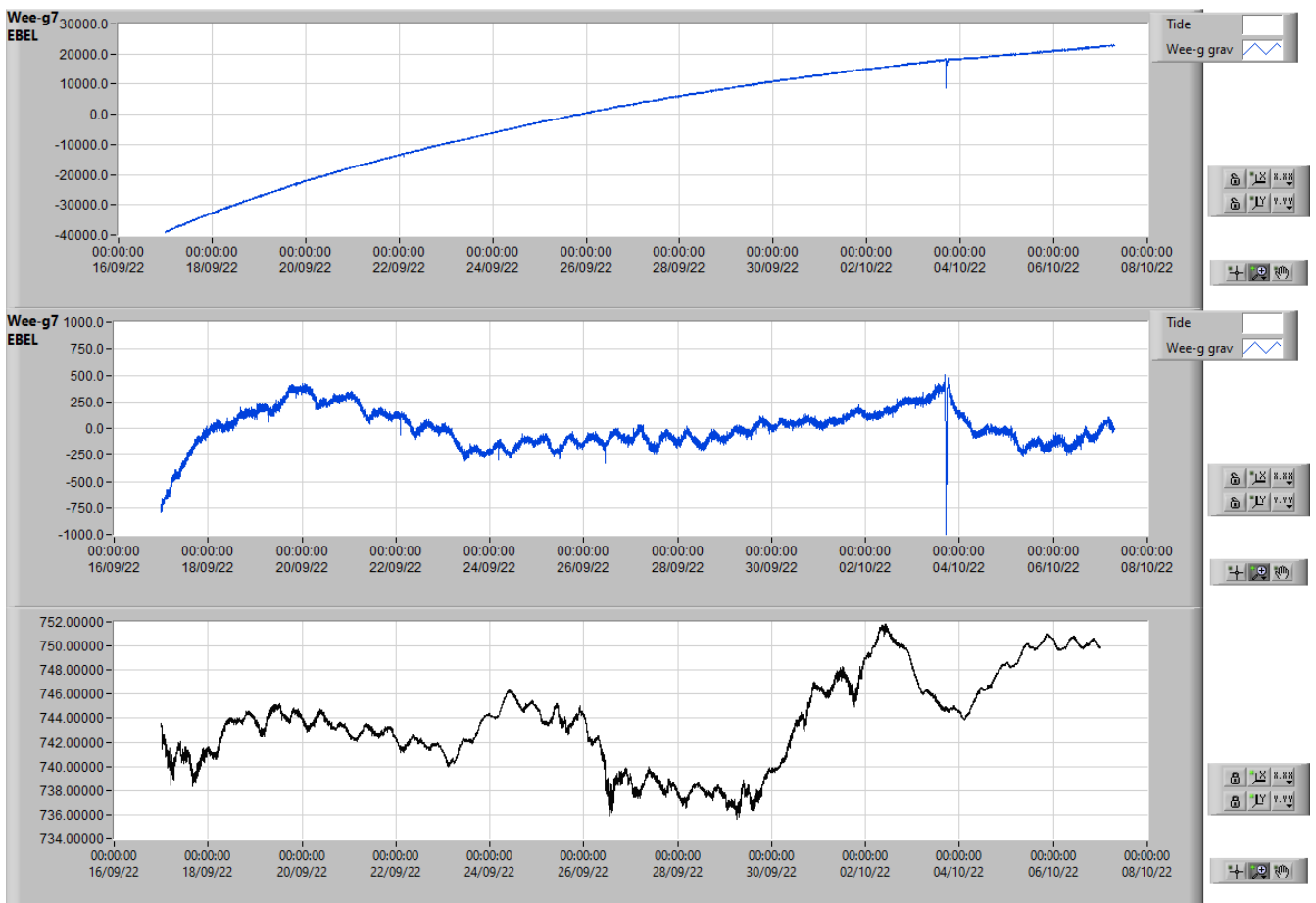


Figure 7 - Wee-g7 at EBEL. Top: raw gravity data. Middle: gravity data after removal of a 3rd-degree polynomial fit. Bottom: Pressure

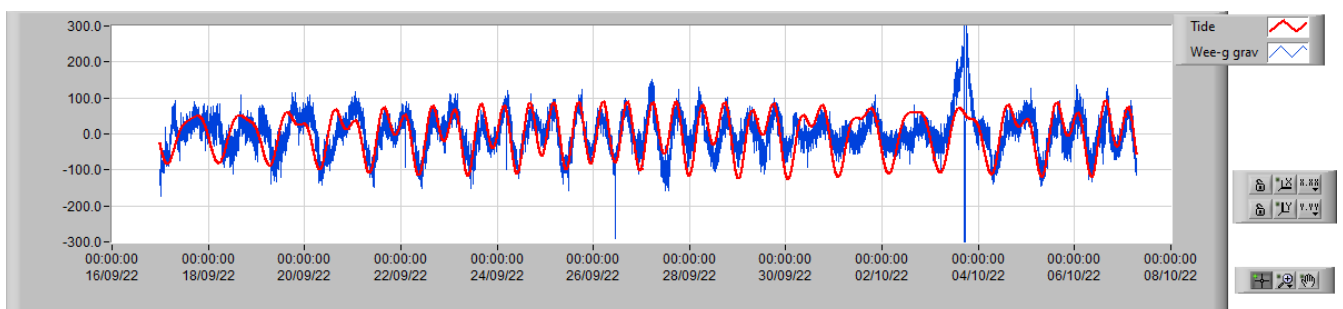


Figure 8 - Wee-g7 at EBEL. Band-pass filtered gravity data (blue) and Earth tide model (red).

3.4 Wee-g6 (ECPN station)

Wee-g6 at ECPN (Fig. 1) lost its thermalisation on 30/08/2022, due to a transient interruption of the power supply during an intervention on the station. The device was re-thermalized on 14/09, but, since then, the signal is affected by frequent negative spikes, that make it practically unusable. Hence, only the signal between 01 and 30 August 2022 is considered in the following. The signal is affected by a drift whose linear component is on the order of 700 μ Gal/day (Fig. 9).

Most of the long-term component is removed once the best-fit 2nd-order polynomial is subtracted (residuals within +/- 200 μ Gal). Direct correlation seems to exist with atmospheric pressure. Again, the correlation between band-pass filtered gravity signal and Earth tide is poor, never higher than 0.7 (Fig. 10).

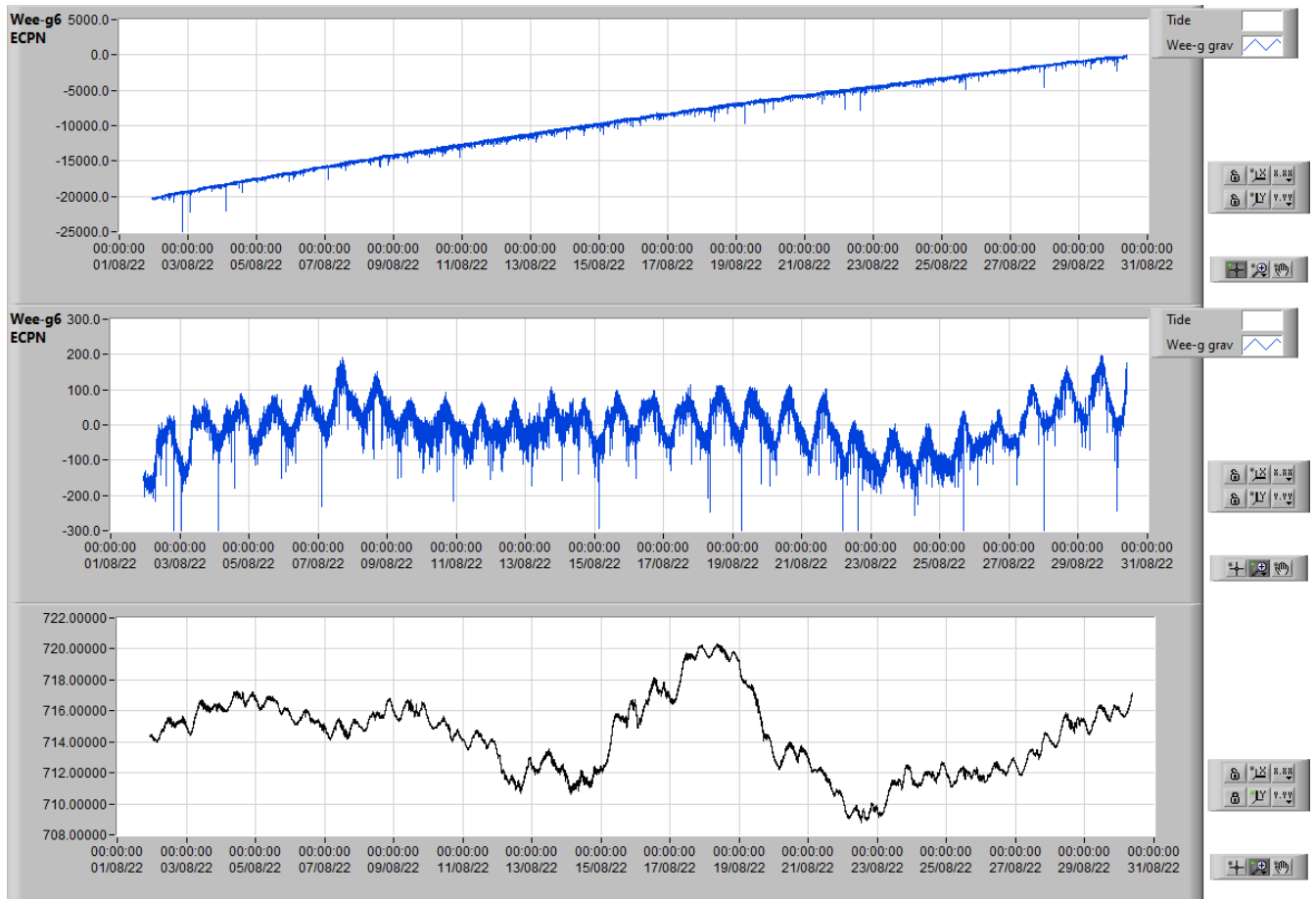


Figure 9 - Wee-g6 at ECPN. Top: raw gravity data. Middle: gravity data after removal of a 2nd-degree polynomial fit. Bottom: Pressure

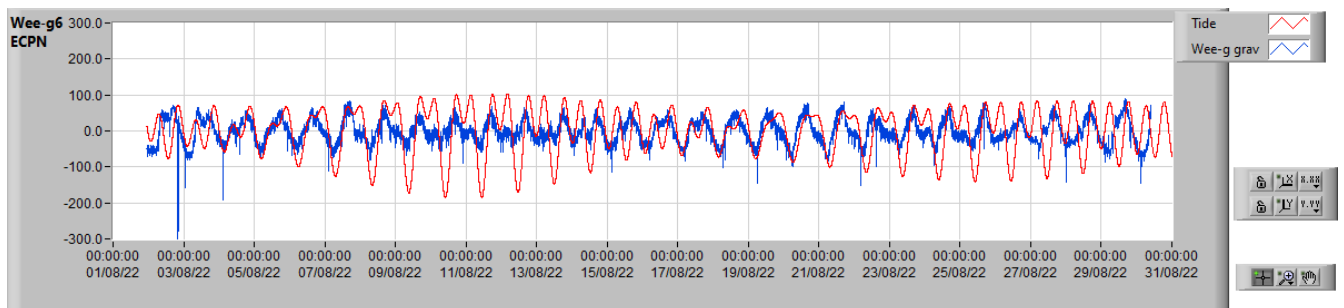


Figure 10 - Wee-g6 at ECPN. Band-pass filtered gravity data (blue) and Earth tide model (red).

3.5 General remarks

Some characteristics of the signals from the Wee-gs installed on Mt. Etna are reported in Table 1. The linear component of the instrumental drift affecting the different signals has a rate ranging between 80 and 3000 μ Gal/day.

The four instruments are differently affected by atmospheric pressure: the maximum absolute value of the admittance (amplitude ratio) ranges between 10 and 300 μ Gal/mbar (Fig. 11).

The Earth tide signal is tracked with different precision by the 4 devices. While RP1.1 is able to quite precisely reproduce the tidal effect at the installation site, Wee-g1 and Wee-g6 only loosely track the gravity changes driven by Earth tide (corr. factor. ≤ 0.7).

Station	Device	Start recording date	End recording date	Drift linear component	Max corr fact with tide	Gravity/pressure max ampl. ratio
SLN	RP1.1	04/09/2021	Running	140 μ Gal/day	0.96	-300 μ Gal/mbar
EPDN	Wee-g1	27/07/2022	Running	80 μ Gal/day	0.70	-80 μ Gal/mbar
EBEL	Wee-g7	17/09/2022	Running	3 mGal/day	0.80	-
ECPN	Wee-g6	01/08/2022	30/08/2022	500 μ Gal/day	0.70	10 μ Gal/mbar

Table 1 – Some characteristics of the signals in output from the Wee-g devices deployed at Mt. Etna.

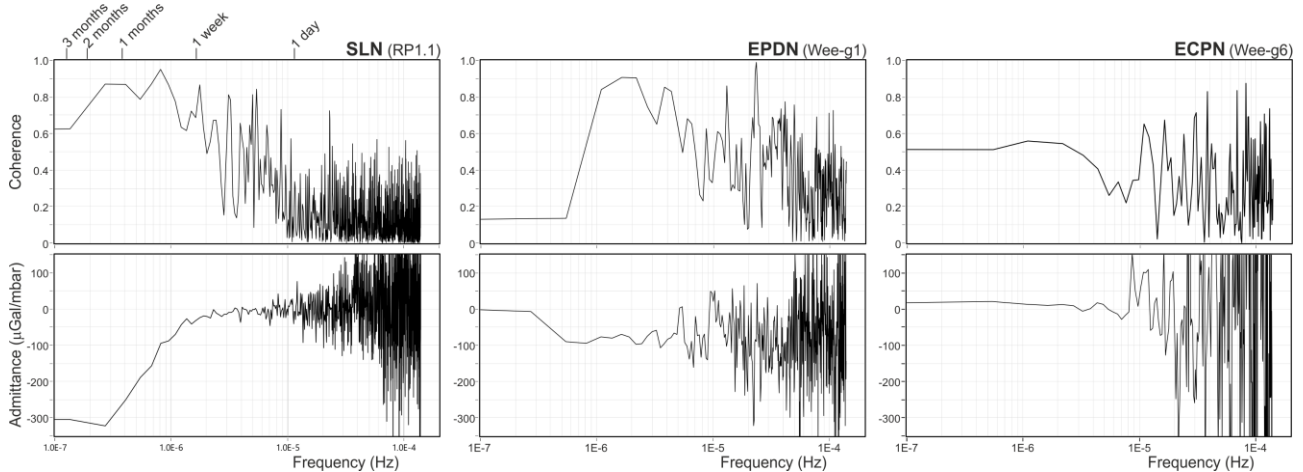


Figure 11 - Cross spectral analyses on Wee-g outputs and atmospheric pressure. Top: coherence plot; bottom: admittance plot. Over the correlated (high coherence) parts, the maximum absolute value of the admittance is about 300 (RP1.1 at SLN), 80 (Wee-g1 at EPDN) and 10 (Wee-g6 at ECPN) μ Gal/mbar.

The different effect of atmospheric pressure on the Wee-g signal is shown in Fig. 12, where the comparison between data from EPDN and ECPN is presented. The higher gravity/pressure admittance induces strongest fluctuations in the signal from EPDN (admittance = -80 μ Gal/mbar) than in the signal from ECPN (admittance = 10 μ Gal/mbar).

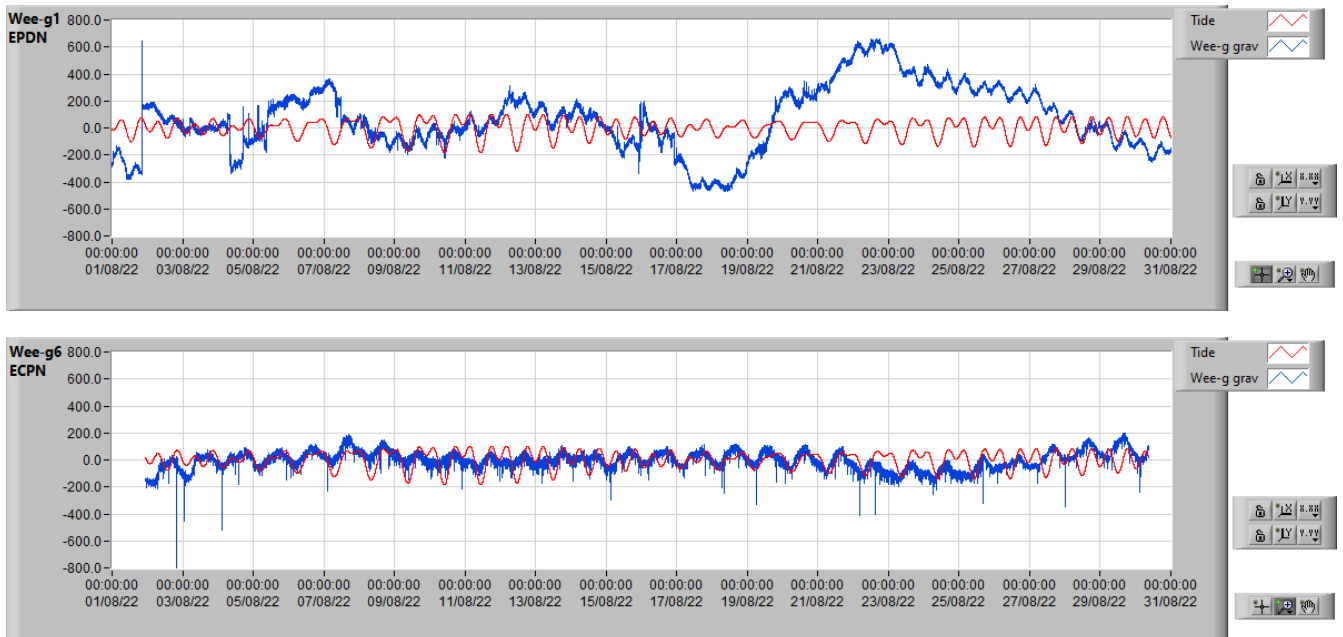


Figure 12 - Gravity data from EPDN (top) and ECPN (bottom), after removal of a low-degree polynomial fit (blue curves). The red curves both represent the Earth tide model. The two plots have the same vertical scale.

The strong and nonlinear drift, including the commonly encountered response to atmospheric pressure changes, makes the detection of standard gravity changes induced by geophysical

processes challenging with Wee-g devices, especially if the changes occur over relatively long time scales. Further improvements are thus needed in order to make the Wee-g suitable for inclusion in measurement systems like the NEWTON-g's gravity imager. Indeed, the results obtained from the deployments at Mt. Etna have spurred several major design changes which will be implemented in the next generation of Wee-g instruments. One of such changes involves a passive temperature compensation strategy that is expected to reduce the temperature sensitivity of the MEMS sensors and, hence, the rate of long term drifts. In particular, composite materials will be utilized for manufacturing the sensor chips, which will help in (i) reducing the temperature sensitivity and (ii) packaging under vacuum the MEMS sensors, through standard hermetic sealing technology. This will most likely eliminate any response to atmospheric pressure changes. UNIGLA is also planning to change the design of the thermal enclosure hosting the sensor. In the new generation of instruments, the vacuum sealed MEMS sensors will be installed within an evacuated metal enclosure that will provide a second layer of isolation from pressure and temperature changes.

Apart from the above planned upgrades, it is worth stressing that exceptional volcano-related gravity changes, like those observed at Kilauea and described by Carbone et al. (2013) and Poland et al. (2021), which involved variations of hundreds of μGal in a matter of hours, would likely be detected by the current version of the Wee-g.

4 Analysis of data from AQG-B03 and comparison with other gravity data

4.1 Introduction

As stated in Section 2, AQG-B03 was reinstalled at PDN (Fig. 1) in late July 2022 and has acquired continuous gravity data ever since. The time series recorded during 20 July to 23 September is shown in panel A of Fig. 13. Data are corrected for environmental effects (Earth tide, polar motion, atmospheric pressure, ground tilt) and the instrumental effects described by Antoni-Micollier et al. (2022). The gaps in the time series are due to temporary failures of the hybrid power supply system of the gravimeter (see D3.4) and to checks that were accomplished to verify the performances of the instrument, after the upgrades accomplished by iXblue in June and early July (see D2.6).

4.2 Comparison with data from other gravimeters on Mt. Etna

The signal produced by AQG-B03 in 2022 is checked against the data from the two iGrav superconducting gravimeters (SGs), which are part of Mt. Etna's monitoring system, managed by INGV-OE (Carbone et al., 2019). The two SGs are located at SLN and at La Montagnola hut (MNT), a site at 2600 m elevation and 3.5 km from the summit craters of Mt. Etna (Fig. 1). The main common features among the signals from the AQG-B (Fig. 13A) and the two iGravs (Fig. 13B and C) are the phases of gravity decrease occurring between (i) late July and mid-August and (ii) late August and mid-September (marked, respectively, with 1 and 2 on top of Fig. 13). The first gravity decrease is also visible in the signal from L&R G-1190 at ECNE (Fig. 13C), but only until early August. Afterwards, instrumental effects, likely driven by external parameters, become predominant (grey part of the curve shown in Fig. 13C) and it is not possible any more to straightforwardly track volcano-related gravity changes using the signal from this instrument.

We use the information on the late July to mid-August gravity changes, retrieved from the AQG-B, the two iGrav SGs and the L&R, to tentatively define the main parameters of the common underground mass source. Instead of simply estimating the amplitudes of the change at each site during the target interval through inspection of the time series, we also calculate the amplitude ratios among couples of signals, using the scatterplots shown in Fig. 13E, F and G. For each scatterplot, the slope of the best-fitting line is taken as the amplitude ratio between the two time series involved in the calculation. The final value of the gravity change at each site is thus defined through cross-analyzing the amplitude ratios and the values retrieved directly from the time series (Table 2).

4.3 Data inversion

The gravity data reported in Table 2 are inverted to define the position of the common source and the amount of redistributed mass, under two a-priori assumptions: (1) there was only negligible large-scale deformation during the studied period; (2) the observed gravity changes were induced by an isotropic point-source (Mogi model). The best fit to the measured gravity changes is calculated by minimizing the sum of absolute deviations (SAD), for a given set of source parameters (source

position and mass change).

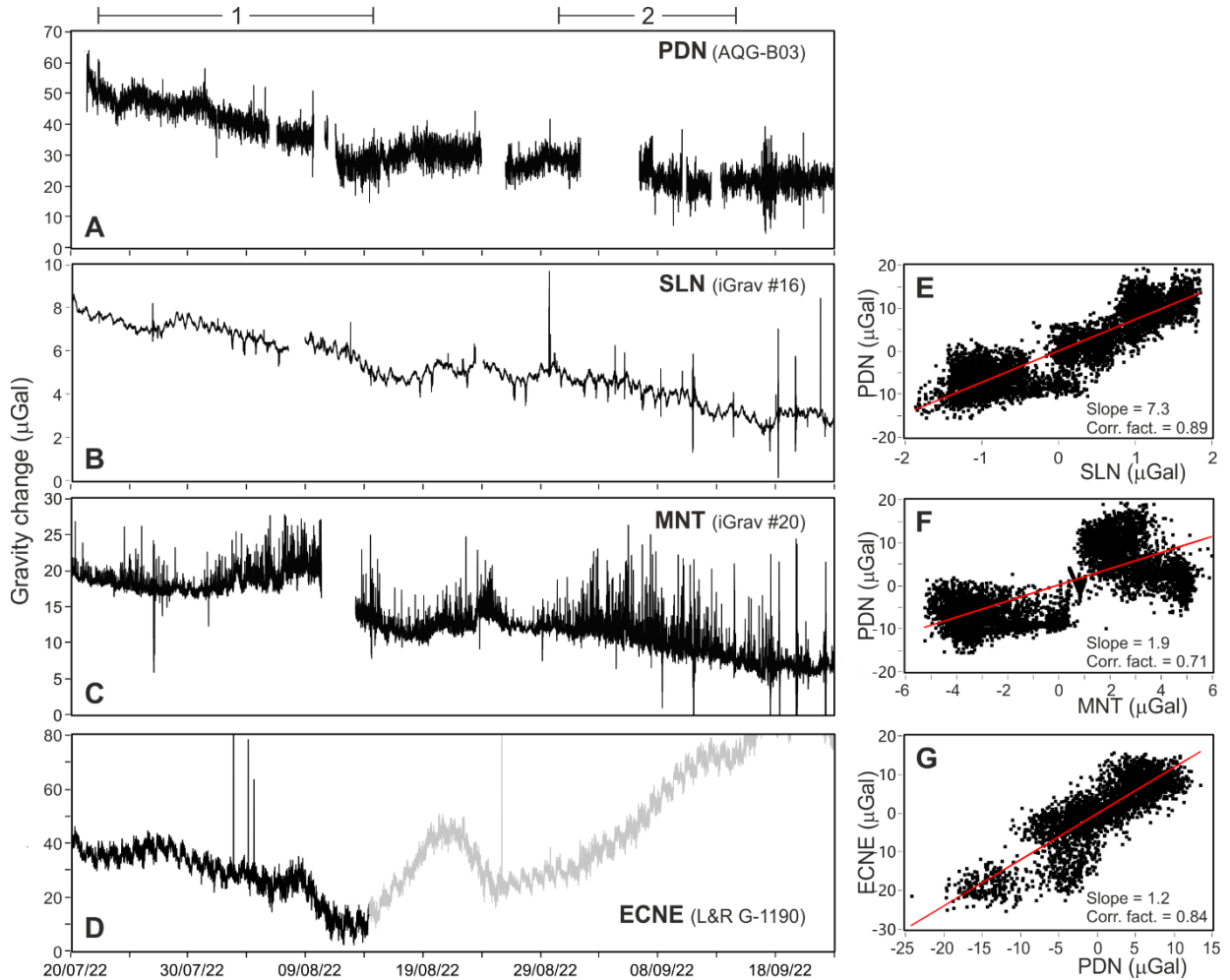


Figure 13 - Gravity time series from (A) AQG-B03 at PDN; (B) iGrav#16 at SLN; (C) iGrav#20 at MNT; (D) L&R G-1190 at ECNE, during 20 July to 23 September 2022. Signals in A, B and C are corrected for all environmental perturbations and, in the case of the AQG-B, also for possible instrumental effects. The signal in D is corrected only for the effect of Earth tide and atmospheric pressure, while possible effects driven by tilt changes or instrumental drift are not accounted for. E, F and G show scatterplots of, respectively, SLN against PDN, MNT against PDN and PDN against ECNE. For each scatterplot, the slope of the best-fitting line and the correlation coefficient are reported. The segments labelled 1 and 2 on top of the left block mark the two main phases of gravity decrease.

Station / device	Obs. change (μGal) late July - mid-August	Amplitude ratios (Fig. 13C, D, E)	Calc. Change (μGal) (optimal solution)
PDN / AQG-B03	-20.0		-19.92
SLN / iGrav#16	-2.8	PDN/SLN = 7.3	-2.83
MNT / iGrav#20	-10.0	PDN/MNT = 1.9	-10.67
ECNE / L&R G-1190	-24.0	ECNE/PDN = 1.2	-23.89
Parameters of the optimum solution			
East (m)	North (m)	Depth (m b.s.l.)	Mass change (kg)
499825	4178550	1125	-6.67 * 10 ¹⁰

Table 2 – Top part: gravity changes observed at PDN, SLN, MNT and ECNE during late July to mid-August (2nd column from left), defined through cross-analyzing the amplitude ratios (3rd column) and the values retrieved directly from the time series. The gravity changes calculated using the parameters of the optimal solution are also shown (4th column). Bottom part: parameters (location and involved mass change) associated with the optimal solution.

The optimum solution is uniformly searched in a 3 x 3 x 3 km³ volume around and beneath the summit craters. Fig. 14 shows the position of the optimum solution and the 100 solutions allowing the lower values of SAD. The optimum solution is located beneath the summit craters, at depth of

about 1100 m b.s.l. (Fig. 14). The other solutions corresponding to the lower values of SAD cluster around the optimum solution (Fig. 14), which confirms the reliability of the result. The mass change providing the best fit to the observed gravity changes is $-6.7 \cdot 10^{10}$ kg (Table 2). This mass decrease could reflect an increase in magma vascularity within a reservoir at the inferred depth. For example, assuming an unidimensional reservoir with size of ~ 1 km, the above mass decrease implies an increase in vascularity of about 5%.

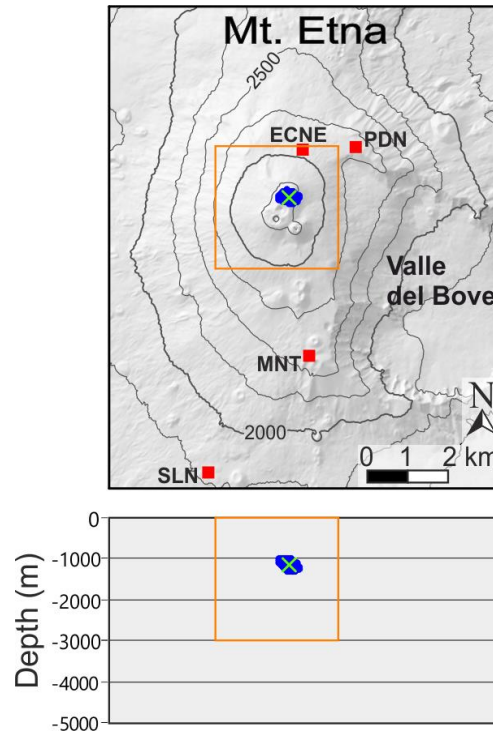


Figure 14 – Results from the gravity data inversion shown on the map (top) and on a E-W cross section (bottom). The green cross marks the position of the optimum solution, while the blue dots mark the positions of the 100 solutions allowing the lower values of SAD. The red squares are the stations where the data used in the calculation were recorded. The orange box defines the volume over which the optimum solution was uniformly searched.

5 Concluding remarks

One of the main targets of NEWTON-g has been demonstrating the potential of continuous gravimetry performed through an extended array of observation points. The NEWTON-g's concept of gravity imager involves an array of lower-cost and lower-resolution gravimeters (MEMS devices), whose signals are referenced to the signal from a more expensive gravimeter, featuring high sensitivity and long-term stability at the μGal level (the AQQ-B).

Unfortunately, despite the important advancements that the UNIGLA-IGR team has made on the development of the Wee-g MEMS gravimeter in the frame of the project (see D2.2, D2.5, D2.6), it has not yet been possible to attain the detection performance needed to measure gravity changes induced by geophysical processes (a few to a few hundreds of μGal , over time-scales of hours to years). More effort will thus be necessary (also beyond NEWTON-g) to further push the Wee-g along the technology readiness level scale (see section 3.5).

The successful integration of the AQQ-B in the existing Mt. Etna's infrastructure for continuous gravity monitoring (Carbone et al., 2019) has demonstrated that, if data from an array of instruments featuring sufficient precision and long-term stability are available, real time detection of volcano-related anomalies, occurring over time scales of days to months, can be performed and unique indications on the characteristics of the common mass source can be obtained (section 4), even during quiescent periods. This is especially true if data from gravimeters at closer distance from the active structures are also available. As shown in section 4, by comparing the signal from L&R G-1190 with the signals from the AQQ-B and iGrav SG devices, it is possible to isolate, in the time

series produced by the spring gravimeter, a part which is less affected by instrumental effects and can thus be used to further constrain the characteristics of the underground mass source at work. Data from the more stable devices could be also used to inform non-linear algorithms aimed at reducing the gravity signal from spring or MEMS gravimeters for the instrumental effect induced by ambient perturbations (e.g., Andò and Carbone, 2006).

Finally, it is worth stressing that, while most of the NEWTON-g data remain under embargo, the consortium has made data from the AQQ-B at PDN, collected during August to November 2020 (Antoni-Micollier et al., 2022), publicly available, following conventional mSEED data standards and FAIR principles. These data were uploaded to the European Integrated Data Archive (EIDA) and can be downloaded through the ORFEUS Data Center FDSN web services using network identifier 2Q and station identifier AQQ (see: <http://orfeus-eu.org/fdsnws/dataselect/1/>). The integration with existing data infrastructures and standards makes the NEWTON-g data findable and accessible to a wide scientific audience.

References

- Andò, B., Carbone, D., 2006. A new computational approach to reduce the signal from continuously recording gravimeters for the effect of atmospheric temperature. *Phys. Earth Planet. Inter.* 159 (3–4), 247–256. <http://dx.doi.org/10.1016/j.pepi.2006.07.009>.
- Antoni-Micollier, L., Carbone, D., Ménoret, V., Lautier-Gaud, J., King, T., Greco, F., et al., 2022. Detecting volcano-related underground mass changes with a quantum gravimeter. *Geophysical Research Letters*, 49, e2022GL097814. <https://doi.org/10.1029/2022GL097814>.
- Carbone, D., Poland, M.P., Patrick, M.R., Orr, T.R., 2013. Continuous gravity measurements reveal a low-density lava lake at Kīlauea Volcano, Hawai'i. *Earth Planet. Sci. Lett.*, 376, 178–185. <http://dx.doi.org/10.1016/j.epsl.2013.06.024>.
- Carbone, D., Cannavò, F., Greco, F., Reineman, R., Warburton, R. J., 2019. The benefits of using a network of superconducting gravimeters to monitor and study active volcanoes. *Journal of Volcanology and Geothermal Research*, 124, 4035–4050. <https://doi.org/10.1029/2018jb20017204>
- Carbone, D., Antoni-Micollier, L., Hammond, G., de Zeeuw - van Dalssen, E., Rivalta, E., Bonadonna, C., et al., 2020. The NEWTON-g gravity imager: Toward new Paradigms for terrain gravimetry. *Frontiers of Earth Science*, 8, 573396. <https://doi.org/10.3389/feart.2020.573396>.
- Poland, M.P., Carbone, D., Patrick, M.R., 2021. Onset and evolution of Kīlauea's 2018 flank eruption and summit collapse from continuous gravity. *Earth and Planetary Science Letters*, 567, 117003. <https://doi.org/10.1016/j.epsl.2021.117003>.